SCIENTIFIC REPORTS

OPEN

SUBJECT AREAS:
PHYSICS
MATERIALS SCIENCE
SPECTROSCOPY
ANALYTICAL CHEMISTRY

Received
7 August 2012

Accepted
26 September 2012

Published
14 November 2012

Correspondence and requests for materials should be addressed to M.O. (m.ohkubo@aist.go.jp)

X-ray absorption near edge spectroscopy with a superconducting detector for nitrogen dopants in SiC

M. Ohkubo[1], S. Shiki[1], M. Ukibe[1], N. Matsubayashi[1], Y. Kitajima[2] & S. Nagamachi[3]

[1]Research Institute of Instrumentation Frontier (RIIF), National Institute of Advanced Industrial Science and Technology (AIST), Tsukuba Central 2, 1-1-1, Umezono, Tsukuba, Ibaraki, 305-8568, Japan, [2]Photon Factory (PF), Institute of Materials Structure Science, High Energy Accelerator Research Organisation (KEK), 1-1, Oho, Tsukuba, Ibaraki, 305-0801 Japan, [3]Ion Technology Centre Co., Ltd., Tsuda Science Hills, 2-8-1 Tsudayamate, Hirakata-shi, Osaka, 573-0128 Japan.

Fluorescence-yield X-ray absorption fine structure (FY-XAFS) is extensively used for investigating atomic-scale local structures around specific elements in functional materials. However, conventional FY-XAFS instruments frequently cannot cover trace light elements, for example dopants in wide gap semiconductors, because of insufficient energy resolution of semiconductor X-ray detectors. Here we introduce a superconducting XAFS (SC-XAFS) apparatus to measure X-ray absorption near-edge structure (XANES) of *n*-type dopant N atoms (4×10^{19} cm^{-3}) implanted at 500°C into 4H-SiC substrates annealed subsequently. The XANES spectra and *ab initio* multiple scattering calculations indicate that the N atoms almost completely substitute for the C sites, associated with a possible existence of local CN regions, in the as-implanted state. This is a reason why hot implantation is necessary for dopant activation in ion implantation. The SC-XAFS apparatus may play an important role in improving doping processes for energy-saving wide-gap semiconductors and other functional materials.

It is known that the doping of light elements into wide-gap semiconductors is difficult compared with Si. This difficulty is caused by the fact that, in wide-gap semiconductors, dopant atoms can possibly occupy several substitution sites and moreover lattice damage recovery is complex. Among wide-gap semiconductors, ion implantation doping into SiC is feasible up to a point[1,2]. SiC is, therefore, the leading material for practical products such as Schottky barrier diodes and field effect transistors[1]. However, 100% dopant activation cannot be obtained at N concentrations of higher than the critical dose of $\sim 10^{19}$ cm^{-3} [2,3]. The incomplete dopant activation, which leads to high resistance, counteracts the low power loss due to the intrinsic material properties. Furthermore, it is even controversial which of the Si and C sites in SiC can be substituted by the N dopant. More seriously, ion implantation doping has not yet been established in other materials such as ZnO, GaN and diamond.

One critical hurdle is that no analytical method for atomic-scale local structures has been realised for trace light elements in matrices[4]. Transmission electron microscopy can visualise individual dopant atoms, for example, Sb in Si[5] and Y in Al_2O_3[6], but it is limited to heavy elements in light matrices. Three-dimensional tomographic atom probe seems not to have enough spatial resolution for fixing substitution sites[7,8]. Scanning probe microscopy can image dopant atoms, but it is difficult to obtain site information[9]. Dopant site occupation has been studied by electron paramagnetic resonance, electron nuclear double resonance and nuclear magnetic resonance spectroscopy[10,11]. However, because these techniques require bulk samples, they are unsuitable for ion-implanted surface layers. The only possible technique for solving this problem may be X-ray absorption fine structure (XAFS) spectroscopy.

Fluorescence-yields (FYs) obtained by scanning monochromatic synchrotron radiation (SR) energy provide a method for measuring the XAFS spectra of specific trace elements[12]. However, conventional semiconductor energy-dispersive-X-ray (EDX) spectroscopy can insufficiently cover the soft X-ray region below 1 keV[13], in which the *K* lines of light elements such as Li, B, C, N and O are present. Although the latest Si drift detector recorded an excellent energy resolution (ΔE) of 48 eV in full width at half maximum (FWHM) for the O–*K* line (525 eV)[14], it is difficult to separate the weak N–*K* line from the strong C–*K* line tail in N-doped SiC samples, because the C–*K* edge energy of 284 eV is lower than the N–*K* edge energy of 410 eV. For that purpose, an energy resolution of better than $\sim$15 eV is desirable to eliminate the C–*K* line disturbance.

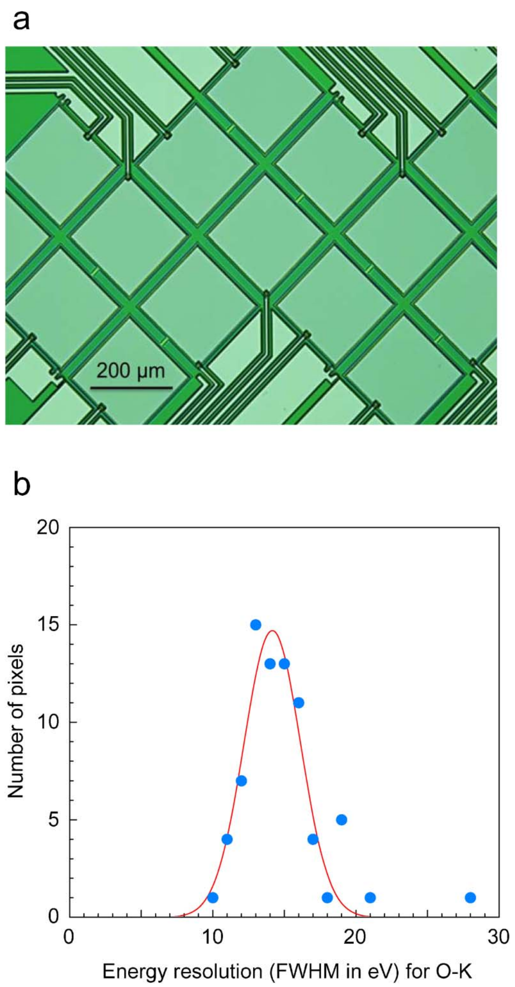

Figure 1 | Superconducting X-ray detector. (a) Close-up of the 100 pixel array detector with 200-µm-square superconducting-tunnel-junctions (STJs). Because of the better energy resolution (ΔE), an array detector of 100-µm-square pixels with the same arrangement was used to measure XANES of N in SiC. (b) Histogram of ΔE values for the 80 operating 100-µm-square STJs. The solid line shows a Gaussian fit with a mean value of 14.2 eV and a standard deviation of 2.8 eV.

Superconducting detectors overcome the theoretical limit of semiconductor detectors[15]. Superconducting tunnel junction (STJ) array detectors are suitable for bright SR beams because of an acceptable high flux of over 20 k photons/s per pixel with sufficient ΔE values of 8–15 eV depending on the junction size, junction layer structure, and superconductor materials[13,16]. A group at the Lawrence Livermore National Laboratory pioneered FY–XAFS spectroscopy with STJ detectors[13]. However, to date, the application to semiconductors has been limited to our report on an N-doped ZnO sample (3×10^{20} cm^{-3})[17]. In ZnO, the X-ray absorption near edge structure (XANES) spectra, which are sensitive to the three-dimensional arrangement of atoms in space, were used to locate the N substitution site and also indicate N_2 formation after annealing. In contrast to N-doped SiC, no strong background from the matrix at the SR beam energy of the N *K*-edge exits in the N-doped ZnO, since the N *K*-edge is lower than the O *K*-edge. In this study, the performance of the SC-XAFS instrument was improved to analyse N-doped SiC.

Results

Figure 1a shows a close-up photograph of the 200-µm-square Nb–Al STJ pixels in the superconducting detector. An array detector with 100-µm-square STJs were also fabricated. The pixel number distribution as a function of ΔE for the O-*K* line in the 100-µm-square STJs is plotted in Fig. 1b. The current SC-XAFS system has the largest operating pixel number to the best of our knowledge. The distribution is narrow and within 10–20 eV: a standard deviation of 2.8 eV was associated with a mean ΔE value of 14.2 eV that is enough for separation of the *K* lines of the adjacent light elements. The ΔE values were limited by the read-out electronic noise of typically 10 eV, so that the theoretical ΔE limit[18] of ~2 eV for the O-*K* line could not be attained at this moment. The ΔE values for the 200-µm-square pixels were only slightly better than that of the Si drift detector, although they had a larger sensitive area. Therefore, the 100-µm-square STJ array detector was used in this study.

An example of the fluorescence spectra at an SR beam energy of 453 eV for the 4H-SiC sample in the as-implanted state (4×10^{19} N atoms cm^{-3}) is shown in Fig. 2. The spectra of the 80 operating STJ pixels were integrated. Inappropriately, the first- and second-order SR beams are recognised as a consequence of elastic scattering. In addition, the second-order SR beam produces the O-*K* peak that may originate from an oxidised surface layer. In the linear scale plot shown in the inset, only C-*K* peak is recognised, whereas in the log scale plot, the SC-XAFS apparatus enables the extraction of the weak N-*K* peak from the spectral complexity.

Figure 3a shows the XANES spectra after background subtraction with the energy window shown in Fig. 2 for three samples: as-implanted at 500°C, annealed at 1400°C, and annealed at 1800°C. It has been well known that ion implantation at elevated temperatures is critical for high-dose doping in SiC[2], but there is no report on local structures of implanted dopants and thus the cause has not been known. In all XANES spectra, peaks and bumps are recognised at 405 eV and 420 eV. The shapes slightly change with annealing; in particular, the small oscillations observed above 425 eV in the as-implanted sample disappear after annealing. The origin of this change is unclear, but it may be related to N-defect pairs[19], stacking faults forming quantum wells in the 4H matrix[20] or other extended defects formed by post-annealing. In fact, it has been confirmed by the ion channeling measurements described below that interstitial atoms induced by the ion implantation are reduced by annealing at 1400 and 1800°C, so that remaining detects should have some orders.

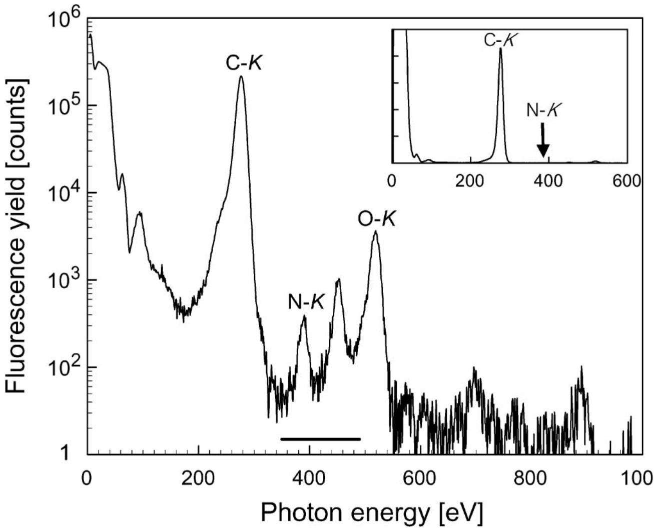

Figure 2 | Fluorescence spectrum at a probe energy of 453 eV for the 4H-SiC after N implantation at 500°C and a dose of 4×10^{19} cm^{-3}. The data for the 80 operating pixels were integrated. The O-*K* peak was produced by the second-order SR beam at 906 eV. The peak at 700 eV may be assigned to the Fe-*L* line due to a material surrounding the sample. The bar near 400 eV shows the energy window for the XANES spectra in Fig. 3. The inset shows a linear scale plot.

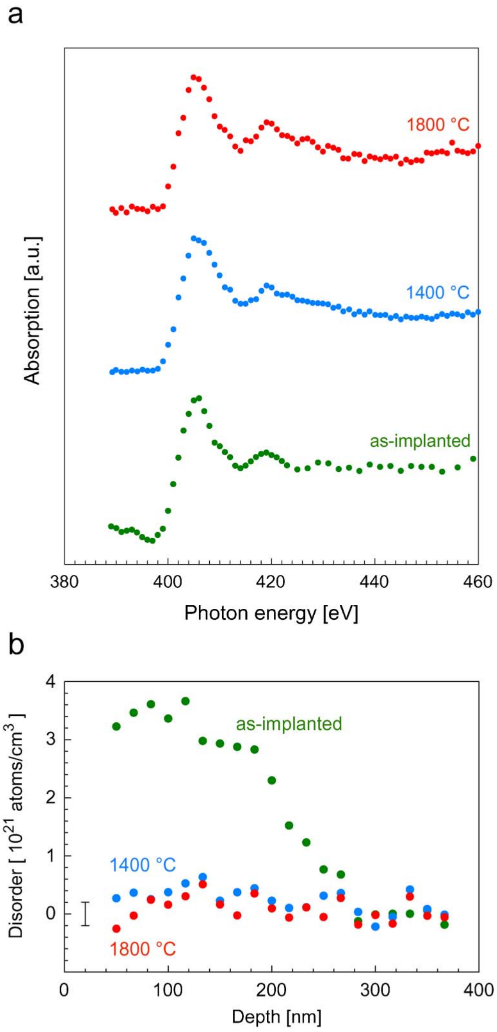

Figure 3 | XANES spectra and lattice disorder. (a) XANES spectra in the as-implanted state and after annealing at 1400°C or 1800°C. (b) Lattice disorder calculated from He$^+$ ion channeling yields of the Si atoms. The error bar is indicated by the vertical solid line.

The small structure below 400 eV for the as-implanted sample in Fig. 3a also disappears after annealing. In CN samples, the structure in this energy range, which is assigned to $1s \rightarrow \pi^*$ transitions show evidence of C-N bonds[21]. It is possible that local CN regions are formed after the N implantation at 500°C in the disordered state revealed by the ion channeling measurements. No structure below 400 eV was observed in the Si-N bond in SiN[22]. It is, therefore, reasonable that the CN regions disappear and only Si-N bonds remain after annealing.

The lattice damage and annealing recovery measured by the He$^+$ ion channeling is shown in Fig. 3b. The lattice disorder after the N implantation is approximately 3×10^{21} cm^{-3}, and recovers to the virgin level after annealing at 1800°C. A slight but meaningful disorder remains after annealing at 1400°C. The ion channeling is affected predominantly by the atoms displaced from lattice sites, which are point defects such as interstitials. It is less sensitive to extended defects like staking faults or long-range modulations[23] that have only small effect on the continuous atomic rows. Therefore, the lattice disorder in Fig. 3b represents mostly interstitial atoms displaced from the lattice sites.

Discussion

In order to discuss the substitution sites of N, *ab initio* multiple scattering calculations in Fig. 4a were performed using FEFF8.4[24] with the XANES, full multiple scattering (FMS) and self-consistent field (SCF) cards for the N substitution of the Si and C sites in the 4H and 3C polytypes shown in Fig. 4b, including the two non-equivalent sites either for Si and C in the 4H polytype. It was assumed that the lattice cell was the same as that of the non-doped SiC. The scattering potentials were calculated self-consistently with cluster sizes between 27 and 295 atoms that cover spheres of 0.4–0.9 nm in radius, including the Hedin–Lundqvist/Quinn self-energy for excited states. The convergence of the calculation was obtained in all cases. The calculation results and the conclusion of this report were not meaningfully affected by the cluster sizes. The FEFF calculations for the C-site substitution seem to fit to the experimental XANES spectra.

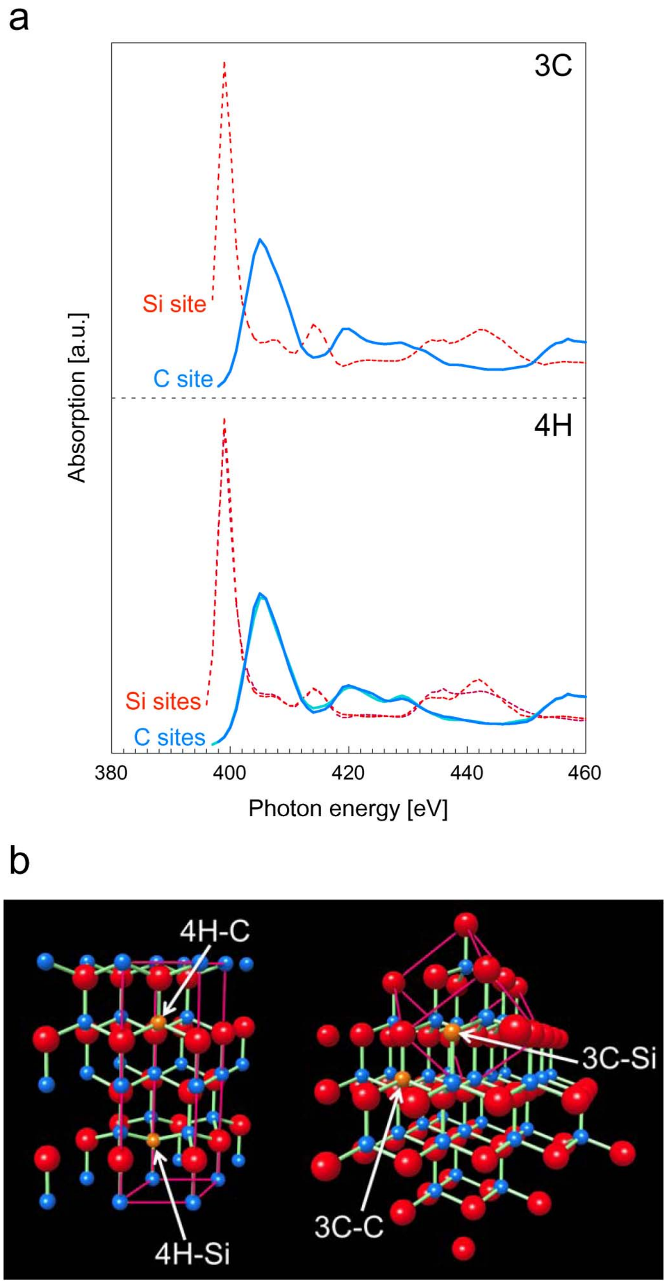

Figure 4 | *Ab initio* multiple scattering calculations. (a) XANES spectra calculated with FEFF8.4[24] for the N atoms in 4H- and 3C-SiC. The difference between the Si and C sites is apparent, whereas the spectra for 4H and 3C are nearly the same. (b) Crystal structure models of the N-doped 4H- and 3C-SiC with possible substitution sites indicated by the arrows. The solid lines show one-fourth of the 4H hexagonal unit cell and the 3C cubic unit cell.

The stacking faults should be considered before further discussion because SiC has approximately 250 polytypes with different stacking sequences of the close-packed Si and C sheets. The polytypes have hexagonal or cubic symmetry, mainly symbolised by 4H and 3C, respectively. In highly N-doped 4H-SiC samples like the present case, a six-layer stacking of the 3C cubic sequence (double layer Shockley fault) appears as a large number of 1.5-nm-thick lamellas parallel to the (0001) basal plane, which is explained by electronically preferable spontaneous transformation during annealing[20,25]. The spontaneous transformation should occur when the annealing temperature is above ~1400°C at the N doping concentration of 4×10^{19} cm^{-3} [20]. The annealing temperature of 1800°C in this study apparently meets this condition. Stacking faults in ion-implanted samples have been routinely reported in the literature[26]. Therefore, the XANES spectra were calculated for both 4H and 3C polytypes. The calculation results, unfortunately, show that the difference between 4H and 3C is extremely small. Nevertheless, according to an FEFF calculation, extended X-ray absorption fine structure (EXAFS) may be accessible for the differentiation between the N atoms in the 4H matrix and the 3C lamellas in the future.

The experimental XANES spectra in Fig. 3a were well reproduced by the FEFF calculations for the N atoms in the C sites either in the 4H or 3C polytypes. The Si site substitution produces totally anti-phase spectra, and thus it is denied. This provides direct evidence that the N atoms substitute for the C sites even in the as-implanted state as well as after post-annealing at high temperatures. Although the possibility of an extremely small percentage of Si-site substitution cannot be rejected, this study has settled the discrepancy in the substitution sites in the literature[10,11,27].

The SC-XAFS data and the FEFF calculations are indicative that the implantation at 500°C results in an almost perfect N substitution of the C site with the point defects and the possible local CN regions, both of which can be removed by post-annealing. The C-site substitution in the as-implanted state is critical for dopant activation in SiC, which is totally different from the doping procedure in Si. The interstitial defects in the SiC sample decrease significantly after annealing at 1400°C, and the residual defects finally relax through the spontaneous 4H-3C transformation at 1800°C. Therefore, the post-annealing is not essential to the substitution of the C lattice site but to the reduction of point defects. The incomplete activation of the dopant is possibly caused by carrier localization in the 3C lamellas, Si vacancies, or N_2 formation, which may be induced from stoichiometric deviation due to the N implantation or Si sublimation. It is suggested that annealing at lower temperatures is required to realise high-dose doping with a 4H single-phase matrix because the critical annealing temperature for the spontaneous transformation decreases as the N dose increases[20]. However, since annealing at low temperatures is ineffective for removing the defects completely, the high dose 4H-SiC may be unrealistic without a non-equilibrium annealing process. Alternative direction for high-performance SiC devices may be using 3C-SiC substrates to realise high dose doping with a 3C single-phase matrix because the lowest band gap among the polytypes prevents the spontaneous transformation.

In conclusion, the present analysis results illustrate that the SC-XAFS apparatus has a significant potential for contributing doping technique development for B, N, Al, and P in SiC and for other wide-gap semiconductors. The combination of SC-XAFS and the FEFF code in the soft X-ray energy range less than 1 keV is versatile for analysing *K*-lines of trace light elements or *L*-lines of impurities that are key components of numerous functional materials also for spintronics, solar cells, and magnetism.

Methods

The details of fabrication, structure and specification of the detector can be found in Supplementary Information. In brief, the SC-XAFS apparatus includes a fully automated 0.3-K cryostat without using liquid He, a cold finger for mounting a detector chip, FET-based charge-sensitive preamplifiers, a digital signal processing system with field programmable gate array (FPGA) chips for 100 pixels and a load-lock for sample exchange[28]. The 80 operating pixels cover a solid angle of approximately 2×10^{-3} sr at a detector–sample distance of 20 mm. The parallel read out circuit system ensures that the acceptable photon flux is well over 1 M photons/s in total. The detector was cooled at 0.3 K, whereas the samples were at room temperature. The SC-XAFS apparatus was installed in the BL-11A beamline (photon fluxes of 10^9–10^{10} photons/s) at the High Energy Accelerator Research Organisation Photon Factory (KEK PF)[29]. Each fluorescence spectrum, which averages the structural information in the entire ion-implanted depth region, at a certain SR beam energy was acquired for 900 s at an interval of 1–2 eV. The XAFS spectra could be monitored on-line by setting an energy window for a specific element, or detailed adjustment of the energy window could be performed off-line for elemental selection and minimisation of the effect of the scattered probe beam in order to obtain reliable XAFS spectra.

Nitrogen ions were implanted at several energies from 10 to 120 keV into a 4H-SiC substrate at 500°C to obtain a flat N distribution at 4×10^{19} cm^{-3}, which is about one order more dilute than in the N-doped ZnO case, in a depth range of 0–200 nm. The dose is also more than the critical dose for the 100% activation. Post annealing was performed at 1400°C or 1800°C for 5 min in an Ar atmosphere.

The ion channeling analysis for the [0001] axis was performed using 2.3-MeV He^{+} ions at a scattering angle of 160°. A comparison between the random and aligned (channeling) spectra for Si atoms provided atomic disorder densities as a function of depth, following a calculation method in ref. 30.

1. Wright, N. Horsfall, A. & Vassilevski, K. Prospects for SiC electronics and sensors. *Mater. Today* **11**, 16–21 (2008).
2. Kimoto, T. Nitrogen ion implantation into α–SiC epitaxial layers. *phys. stat. sol. (a)* **162**, 263–276 (1997).
3. Laube, M. *et al.* Electrical activation of high concentrations of N+ and P+ ions implanted into 4H–SiC. *J. Appl. Phys.* **92**, 549–554 (2002).
4. Castell, M., Muller, D. & Voyles, P. Dopant mapping for the nanotechnology age. *Nature Mater.* **2**, 129–131 (2003).
5. Voyles, P., Muller, D., Grazul, J., Citrin, P. & Gossmann H. Atomic-scale imaging of individual dopant atoms and clusters in highly *n*-type bulk Si. *Nature* **416**, 826–829 (2002).
6. Shibata, N. *et al.* Atomic-scale imaging of individual dopant atoms in a buried interface. *Nature Mater.* **8**, 654–658 (2009).
7. Kelly, T. *et al.* Atom probe tomography of electronic materials. *Ann. Rev. Mater. Res.* **37**, 681–727 (2007).
8. Li, F. *et al.* Laser-assisted three-dimensional atom probe analysis of dopant distribution in Gd-doped CeO_2. *Scrip. Mat.* **63**, 332–335 (2010).
9. Tabe, M. *et al.* Single-electron transport through single dopants in a dopant-rich environment. *Phys. Rev. Lett.* **105**, 016803-1−016803-4 (2010).
10. Son, N., Janzén, E., Isoya, J. & Yamasaki, S. Hyperfine interaction of the nitrogen donor in 4*H*-SiC. *Phys. Rev. B* **70**, 193207-1−193207-4 (2004).
11. Hartman, J. *et al.* NMR studies of nitrogen doping in the 4*H* polytype of silicon carbide: site assignments and spin-lattice relaxation. *J. Phys. Chem. C* **113**, 15024–15036 (2009).
12. Kitajima, Y. Fluorescence yield x-ray absorption fine structure measurements in the soft x-ray region. *Rev. Sci. Instrum.* **66**, 1413–1415 (1995).
13. Friedrich, S. Cryogenic X-ray detectors for synchrotron science. *J. Synchrotron Rad.* **13**, 159–171 (2006).
14. Schlosser, D. Expanding the detection efficiency of silicon drift detectors. *Nucl. Inst. Methods in Phys. Res. A* **624**, 270–276 (2010).
15. Enss, C. *Cryogenic Particle Detection, Topics in Applied Physics 99, Springer, Heidelberg* (2005).
16. Ukibe, M., Ikeuchi, T., Zama, T. & Ohkubo, M. Aluminum thickness dependence of spatial profile in niobium-based superconducting tunnel junctions. *Nucl. Instrum. Methods in Phys. Res. A* **520**, 260–262 (2004).
17. Fons, P. *et al.* Direct observation of nitrogen location in molecular beam epitaxy grown nitrogen-doped ZnO. *Phys. Rev. Lett.* **96**, 045504-1−045504-4 (2006).
18. Kurakado, M. Possibility of high resolution detectors using superconducting tunnel junctions. *Nucl. Instrum. Methods.* **196**, 275–277 (1982).
19. Zvanut, M. & Tol, J. Nitrogen-related point defect in 4H and 6H SiC. *Physica B* **401–402**, 73–76 (2007).
20. Kuhr, T., Liu, J., Chung, H., Skowronski, M. & Szmulowicz, F. Spontaneous formation of stacking faults in highly doped 4H-SiC during annealing. *J. Appl. Phys.* **92**, 5863–5871 (2002).
21. Gago, R. *et al.* Correlation between bonding structure and microstructure in fullerenelike carbon nitride thin films. *Phys. Rev. B* **71**, 125414-1−125414-6 (2005).
22. Baba, Y., Yamamoto, H. & Sasaki, T. Surface x-ray-absorption fine structures of SiO_x ($0<x<2$) and SiN_x ($0<x<4/3$) produced by low-energy ion implantation in Si(100). *Phys. Rev. B* **48**, 10972–10977 (2005).
23. Ohkubo, M. *et al.* Evaluation of individual atomic displacements in mixed atomic rows in Bi-Sr-Ca-Cu-O by ion channeling. *Phys. Rev. B* **54**, 9035–9038 (1996).
24. Ankudinov, A., Nesvizhskii, A. & Rehr, J. Dynamic screening effects in x-ray absorption spectra. *Phys. Rev. B* **67**, 115120-1−115120-6 (2003).
25. Okojie, R. *et al.* Observation of 4H-SiC to 3C-SiC polytype transformation during oxidization. *Appl. Phys. Lett.* **79**, 3056–3058 (2001).
26. Nagano, M. *et al.* Annealing induced extended defects in as-grown and ion-implanted 4H-SiC epitaxial layers. *J. Appl. Phys.* **108**, 013511-1−013511-8 (2010).

27. Kalabukhova, E., Lukin, S. & Mitchel, W. Electrical and multifrequency EPR study of nitrogen and carbon antisite related native detect in *n*-type as-grown 4H-SiC. *Mater. Sci. Forum* **433**, 499–502 (2003).
28. Shiki, S., Ukibe, M., Kitajima, Y. & Ohkubo, M. Fluorescence yield X-ray absorption spectroscopy for O-Kα with elimination of N-Kα background using superconducting tunnel junction detectors. *Physica C* **471**, 1263–1266 (2011).
29. Kitajima, Y. *et al.* Recent performance of the soft X-ray (70–1900 eV) bending magnet beamline 11A at the photon factory. *J. Elec. Spectrosc. Relat. Phenom.* **101–103**, 927–929 (1999).
30. Chu, W., Mayer, J. & Nicolet, M. *Backscattering spectrometry, Academic Press, New York* (1978).

Acknowledgments

This work was partly supported by the Nuclear Research program of the Ministry of Education, Culture, Sports, Science and Technology (MEXT) and the nanotechnology platform program of MEXT (12024046). The measurements at KEK-PF were performed under the approval by the Photon Factory Program Advisory Committee (2009G686 and 2011G678). The authors are grateful to the members of the Super-Spectroscopy Research Group for the experimental assistance, the members of the Clean Room for Analog-Digital Superconductivity (CRAVITY) for the detector fabrication, Y. Gotoh and H. Matsuhata for the information on SiC crystal structures, and M. Koike for his encouragement.

Author contributions

S.N. prepared the SiC samples and performed the ion channeling measurements. S.S. built the SC-XAFS apparatus and performed the XAFS measurements with Y.K. M.U. fabricated the superconducting EDX detector. M.O. planned the research, analysed the data with N.M. and wrote the manuscript. All authors discussed the results and commented on the manuscript.

Additional information

Supplementary information accompanies this paper at http://www.nature.com/scientificreports

Competing financial interests: The authors declare no competing financial interests.

License: This work is licensed under a Creative Commons Attribution-NonCommercial-ShareALike 3.0Unported License. To view a copy of this license, visit http://creativecommons.org/licenses/by-nc-sa/3.0/

How to cite this article: Ohkubo, M. *et al.* X-ray absorption near edge spectroscopy with a superconducting detector for nitrogen dopants in SiC. *Sci. Rep.* **2**, 831; DOI:10.1038/srep00831 (2012).